Efficient Charge Injection from the S_2 Photoexcited State of Special-Pair Mimic Porphyrin Assemblies Anchored on a Titanium-Modified ITO Anode

Mitsuhiko Morisue,[a, b] Noriko Haruta,[a] Dipak Kalita,[a] and Yoshiaki Kobuke*[a]

Abstract: A novel surface fabrication methodology has been accomplished, aimed at efficient anodic photocurrent generation by a photoexcited porphyrin on an ITO (indium–tin oxide) electrode. The ITO electrode was submitted to a surface sol–gel process with titanium *n*-butoxide in order to deposit a titanium monolayer. Subsequently, porphyrins were assembled as monolayers on the titanium-treated ITO surface via phosphonate, isophthalate, and thiolate groups. Slipped-cofacial porphyrin dimers, the so-called artificial special pair at the photoreaction center, were organized through imidazolyl-to-zinc complementary coordination of imidazolylporphyrinatozinc(II) units, which were covalently immobilized by ring-closing olefin metathesis of allyl side chains. The modified surfaces were analyzed by means of X-ray photoelectron spectroscopy. Photoirradiation of the porphyrin dimer generated a large anodic photocurrent in aqueous electrolyte solution containing hydroquinone as an electron sacrificer, due to the small reorganization energy of the dimer. The use of different linker groups led to significant differences in the efficiencies of anodic photocurrent generation. The apparent flat-band potentials evaluated from the photocurrent properties at various pH values and under biased conditions imply that the band structure of the ITO electrode is modified by the anchoring species. The quantum yield for the anodic photocurrent generation by photoexcitation at the Soret band is increased to 15%, a surprisingly high value without a redox cascade structure on the ITO electrode surface, while excitation at the Q band is not so significant. Extensive exploration of the photocurrent properties has revealed that hot injection of the photoexcited electron from the S_2 level into the conduction band of the ITO electrode takes place before internal conversion to the S_1* state, through the strong electronic communication of the phosphonyl anchor with the sol–gel-modified ITO surface.

Keywords: ITO electrode · porphyrinoids · self-assembly · sol–gel processes · special pair

Introduction

Charge injection at an electrode surface is a critical step in the operation of organic molecular electronic devices, such as organic light-emitting diodes, thin-film transistors, and dye-sensitized solar cells.[1] The principal strategy requires a cascade alignment of the energy levels of functional molecules leading smoothly to the Fermi levels of the contact electrode. At the same time, an interfacial dipole at the molecule/electrode junctions alters the charge-injection barriers.[2–4] Manipulation of the surface dipole is thus another important device parameter for tuning the charge-injection efficiency.[5] Also, the electron-transfer rate depends critically on the nature of the chemical linkage.[6,7] The surface chemical modification must offer various manipulable parameters in order to regulate the electron transfer across the molecule/electrode junctions. Surface modification of optically transparent indium–tin oxide (ITO) has thus received much attention due to its practical relevance to organic electronic devices.[3,5]

Molecular engineering in relation to photocurrent generation has provoked a great deal of effort in developing photovoltaics and in emulating natural photosynthetic systems.
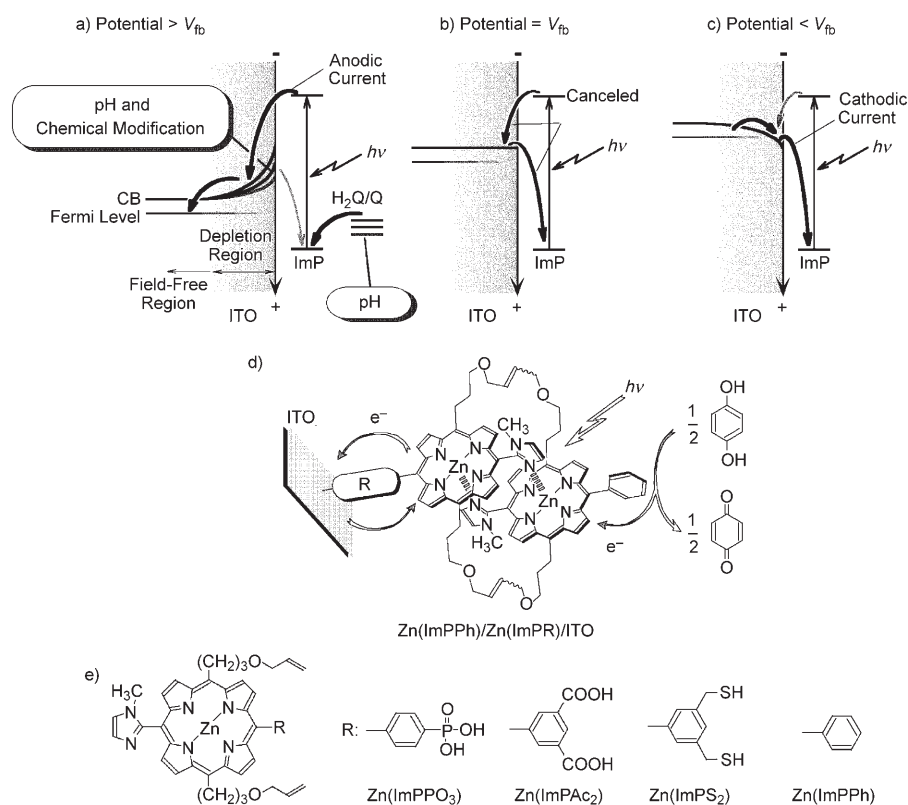
[a] Dr. M. Morisue, N. Haruta, Dr. D. Kalita, Prof. Y. Kobuke
Graduate School of Materials Science
Nara Institute of Science and Technology
8916-5 Takayama, Ikoma, Nara 630-0192 (Japan)
Fax: (+81) 743-72-6119
E-mail: kobuke@ms.naist.jp

[b] Dr. M. Morisue
Present address: Graduate School of Science and Technology
Department of Biomolecular Engineering
Kyoto Institute of Technology
Matsugasaki, Sakyo-ku, Kyoto 606-8585 (Japan)

A precise architecture of the redox cascade on the molecular scale is one of the key factors for achieving an efficient sequential electron-transfer reaction. Therefore, molecular layered systems, such as Langmuir–Blodgett films, self-assembling monolayers (SAMs), and layer-by-layer assemblies, incorporating porphyrins or fullerene, have been employed.[8–11] For the efficient generation of a photocurrent, an ITO electrode is advantageous compared with a gold electrode, since in the latter electron transfer competes with energy-transfer quenching of the excited singlet state by the surface plasmon in the vicinity of the gold surface.[9a,b] The efficiency of photocurrent generation can, in principle, be expected to be enhanced by the ITO system, whereas the quantum yield for the anodic photocurrent on an ITO electrode has been limited to around 20% with even the

Scheme 1. a)–c) Potential diagrams of the surface states of an ITO electrode and redox potentials of the attached porphyrin at various potentials; d) schematic illustration of the "special pair"-mimic porphyrin dimer immobilized on an ITO electrode; e) chemical formulae of imidazolylporphyrins.

most elaborate porphyrin/fullerene/ITO systems.[9c,11b] In contrast, quantum yields for cathodic photocurrent generation on gold electrodes modified with fullerene-terminated SAMs of 50–51% were claimed in the reports of Imahori et al.[8b] and Jen et al.[8c] The molecular systems attached to ITO electrodes for anodic photocurrent generation still remain a limiting factor with regard to improving charge-injection efficiencies.

Despite its high carrier density, ITO is classified as an n-type semiconductor.[12–14] The anodic photocurrent generation system should involve an electron injection from the HOMO of the sensitizer or electron-mediator molecules into the ITO electrode. In this step, the conduction band of the ITO electrode will contribute to the anodic photocurrent generation. The present study aims to evaluate the effect of anchoring group(s) of porphyrin adsorbates on the band structure of an ITO electrode through observing efficient anodic photocurrent generation. Photocurrent efficiencies may reflect differences in charge-injection barriers. On applying high cathodic potentials to ITO, the space charge vanishes and the potential reaches a threshold, at which point the anodic photocurrent falls to zero (Scheme 1a,b). Above the threshold potential, defined as the flat-band potential (V_{fb}), the photocurrent flow is inverted from the anodic to the undesirable cathodic direction (Scheme 1c).[15,16] Therefore, we have explored the photocurrent properties of porphyrin-bearing ITO electrodes in order to

observe possible modification of the charge-injection barriers.

The SAM technique is a facile method for fabricating molecular systems.[17] SAM formation on ITO surfaces using thiol, carboxylate, and phosphonate derivatives is well established.[18] However, the effects of these anchoring groups on electron-transfer processes across the molecule/electrode junctions have not been fully examined, in spite of their utmost importance with regard to the rational design of organic molecular devices. Herein, anodic photocurrent generation efficiencies are compared in order to elucidate the effect of anchoring group(s) on apparent V_{fb} values of a flat ITO electrode under various bulk pH conditions.

Inspired by natural photosynthetic systems, the use of porphyrin SAMs represents a promising basic strategy for the conversion of light energy into an electric current.[8–11] The primary electron donor in natural photosynthesis is constituted by a slipped-cofacial chlorophyll dimer, the so-called "special pair" (SP), at the reaction center.[19] Analogously, two imidazolyl–porphyrinatozinc units, Zn(ImP)s, mutually coordinate through imidazolyl-to-zinc bonds to form a slipped-cofacial dimer as the SP-mimic structure.[20] It has been demonstrated that, due to the delocalization of the radical cation over the two porphyrin rings, the SP-mimic cofacial dimer plays a crucial role in photoinduced electron transfer, by both accelerating charge separation and decelerating charge recombination.[21] Successive self-organization/ring-

closing olefin metathesis processes of Zn(ImP)s on the electrode surface can provide surface-grafted porphyrin assemblies with structural persistence of the organized array.[22] In the present study, a titanium monolayer is deposited by means of a surface sol–gel process. Subsequently, the SP-mimic porphyrin dimer is organized to exhibit efficient photosensitization.

Results and Discussion

Deposition of a titanium monolayer on an ITO surface: An ITO surface was modified as depicted in Scheme 2. Details of the steps are given in the Experimental Section. Reaction of the surface terminal OH groups with metal alkoxides represents a facile method for modifying the nature of the ITO surface.[23–25] Schwartz and co-workers attempted the modification by treating ITO with tetra(*tert*-butoxy)tin and tetra-(*tert*-butoxy)zirconium under ultra-high-vacuum conditions.[23] Similarly, the surface sol–gel fabrication process can provide a molecular metal oxide layer by treatment under mild and ambient conditions.[24] To improve the surface nucleophilicity, the In−OH groups of the ITO surface were converted into Ti−OH groups by sol–gel treatment with titanium tetra-*n*-butoxide (Ti(O*n*Bu)$_4$).[24]

The sol–gel-modified ITO was characterized by using X-ray photoelectron spectroscopy (XPS), and atomic force microscopy (AFM) images were obtained (Figure 1). The Ti-
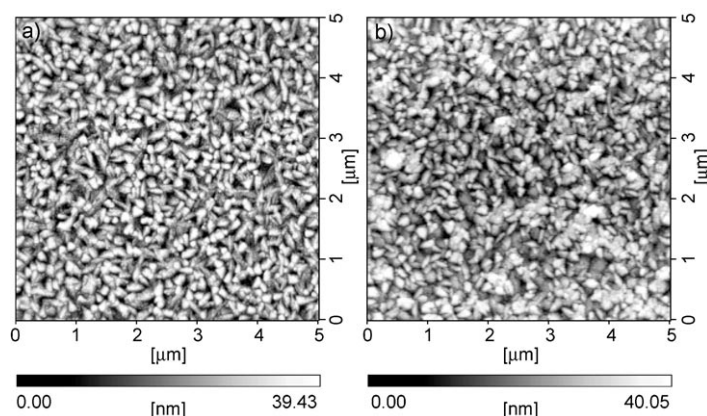

Figure 1. Noncontact mode AFM images of the bare ITO surface (a) and titanium-treated ITO (b).

(2p$_{3/2}$) peaks of titanium oxide are expected to appear at around 454–460 eV in XPS measurements.[26] At the same time, the In(3d$_{3/2}$) peaks appear at around 450–454 eV.[27] Overlap of the In(3d$_{3/2}$) peaks makes it difficult to identify the Ti(2p$_{3/2}$) orbital in the XPS spectra. However, a distinct peak at 531.8 eV was found in the O(1s) region after treatment with Ti(O*n*Bu)$_4$ and hydrolysis (Figure 2b). The shift of the O(1s) binding energy toward higher values suggests that the electron-withdrawing effect of the metal on the oxygen is decreased by the sol–gel process. The increased core binding energy of the oxygen proves that the nucleo-
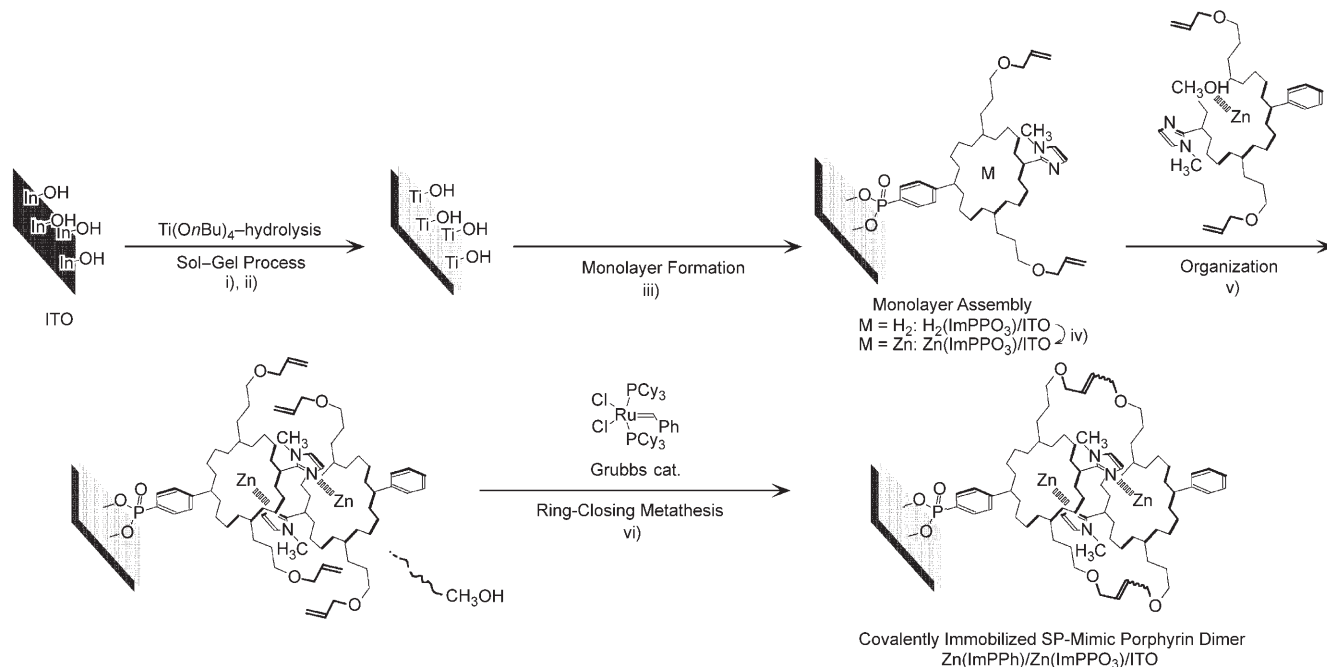
Scheme 2. Procedure for the preparation of the SP-mimic porphyrin dimer on the ITO electrode surface. i) A bare ITO electrode was immersed in 100 mM Ti(O*n*Bu)$_4$ in toluene/ethanol for 3 min. ii) After rinsing thoroughly with ethanol, the ITO was hydrolyzed in water and cleaned by UV/ozone exposure. iii) The titanium-treated ITO was soaked in H$_2$(ImPR) solution under appropriate conditions. iv) Zinc was introduced into the porphyrin in the SAM by immersion in CHCl$_3$ containing an aliquot of saturated Zn(OAc)$_2$ in MeOH at 50 °C for 2 h. v) The SAM-modified ITO was soaked in 1 mM Zn-(ImPPh) in CH$_2$Cl$_2$ containing 20 mM MeOH at room temperature for 24 h, and then rinsed with CH$_2$Cl$_2$ to form the coordination dimer. vi) The coordination dimer was covalently immobilized by soaking in a dilute solution of the Grubbs catalyst at room temperature for 10 min.
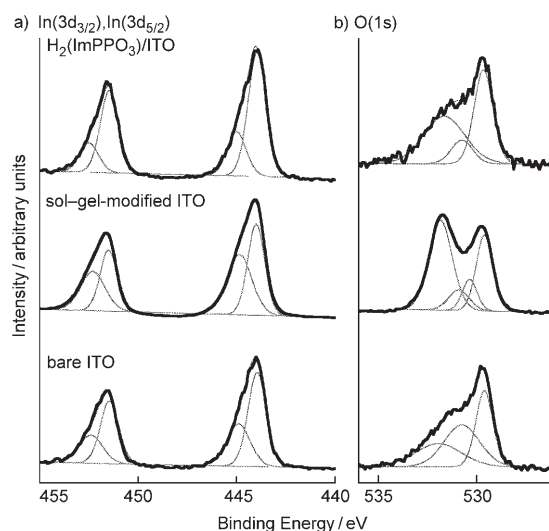
a) In(3d$_{3/2}$),In(3d$_{5/2}$)

H$_2$(ImPPO$_3$)/ITO

b) O(1s)

sol–gel-modified ITO

bare ITO

Binding Energy / eV

Figure 2. XPS-deconvoluted profiles of bare ITO, sol–gel-modified ITO, and H$_2$(ImPPO$_3$)-attached ITO (bottom to top) in the In(3d) region (a) and the O(1s) region (b) observed at a take-off angle of 60°.

philicity of the surface terminal OH groups had been improved. The angular dependence of the photoelectron intensity (Figure 3) is strongly supportive of the location of the
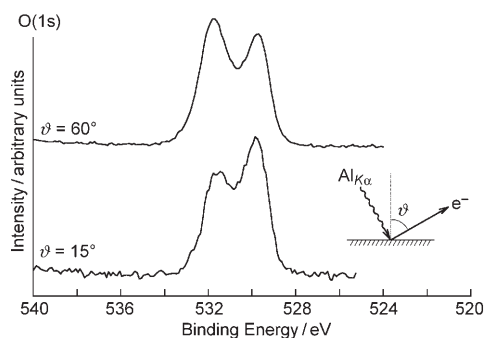
O(1s)

ϑ = 60°

ϑ = 15°

Al$_{K\alpha}$

Binding Energy / eV

Figure 3. Dependence on take-off angle of XPS spectra for the O(1s) region of the sol–gel-modified ITO.

nucleophilic OH groups at the outer terminal positions on the titanium-modified ITO electrode surface. At the same time, inelastic mean free paths cannot completely eliminate the background peak of In(3d$_{3/2}$), suggesting that the thickness of the titanium layer is sufficiently thin as expected (Figure 2a). The disappearance of the peak at 531.8 eV after porphyrin immobilization strongly suggests that the surface nucleophilic terminal OH groups react with the porphyrin anchoring groups (see below). Therefore, the surface sol–gel process led to successful derivatization of the terminal OH groups as required.

Cyclic voltammetry in a buffered aqueous solution showed no charge/discharge process characteristic of a TiO$_2$ semiconductor[28] for the titanium-modified ITO. The absorption spectrum of the titanium-modified ITO showed no detectable change compared with that of the bare ITO in

the UV/visible region (330–850 nm). From this, it can be concluded that the titanium monolayer on the ITO does not possess a band structure with a small energy gap.

The electrochemical behavior of the titanium-treated ITO electrode was characterized by using K$_3$[Fe(CN)$_6$] as a bulk redox probe.[29] No substantial change of the redox couple of bulk K$_3$[Fe(CN)$_6$] was found in the voltammograms by using the titanium-modified ITO working electrodes (see the Supporting Information). From this it can be concluded that the titanium layer does not insulate the redox process between the ITO electrode and the outer redox site.

Organization of the porphyrin dimer as a "special pair" mimic

Zn(ImPPO$_3$) monolayer formation: The ITO glass was immersed in a 1.0 mM solution of H$_2$(ImPPO$_3$) in ethanol at room temperature for 40 h.[30] Thereafter, the substrate was washed with ethanol and dichloromethane, and dried under a stream of nitrogen. The porphyrin incorporated into the SAM was metalated by gently refluxing at 50 °C for 2 h in CHCl$_3$ (4 mL) containing 0.2 mL of a saturated solution of zinc acetate in MeOH.

SP-mimic dimer formation on Zn(ImP)-derivatized ITO: The Zn(ImP)-derivatized ITO electrodes were immersed in 1.0 mM Zn(ImPPh) in CH$_2$Cl$_2$/MeOH (9:1, v/v) for 20 h. Zn-(ImP)s form slipped-cofacial dimers with extremely high association constants (3.3×10^{11} M^{-1}) in noncoordinating solvents through complementary imidazolyl-to-zinc coordination. For organization into a heterodimeric porphyrin with a complementary Zn(ImP) SAM, prior dissociation of the Zn-(ImPPh) unit to the monomer is required. In 1.0 mM Zn-(ImPPh) solution in CH$_2$Cl$_2$, the coordination dimer is partially dissociated by the addition of 20 mM MeOH as a coordinating solvent. During soaking of the SAM-modified ITO electrode for 24 h, the dissociated Zn(ImPPh) was organized into the dimer on the Zn(ImP) SAM as a result of the complementary coordination. The ITO substrate was then rinsed with CH$_2$Cl$_2$ to decrease the MeOH ratio so as to drive the formation of the SP-mimic porphyrin heterodimer on the ITO electrode. The organized structure was covalently fixed through ring-closing metathesis of the allyl side chains by immersion in a dilute solution of the Grubbs catalyst in CH$_2$Cl$_2$ for 10 min. Thorough washing with MeOH and CH$_2$Cl$_2$ removed Zn(ImPPh) molecules adsorbed on the substrate. The SP-mimic porphyrin dimer was thus constructed on the ITO electrode by the organization/metathesis protocol. This methodology has already been established for the construction of structurally robust, surface-grafted multiporphyrin arrays.[22]

Each free-base porphyrin on the ITO electrode showed the Soret band at 421–422 nm, which shifted to 424–426 nm after the incorporation of zinc (Figure 4; see also Figures 7 and 12). The Q band at 516 nm, attributed to the free-base porphyrin, was shifted to 550 nm, indicating that zinc had been incorporated as the central metal ion in the monolayer
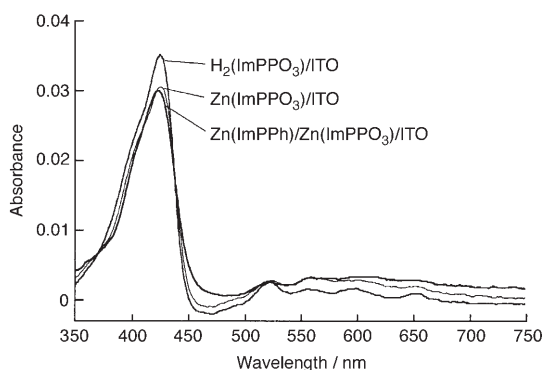
Figure 4. Absorption spectra of H₂(ImPPO₃)/ITO, Zn(ImPPO₃)/ITO, and Zn(ImPPh)/Zn(ImPPO₃)/ITO. These spectra were obtained by background subtraction.
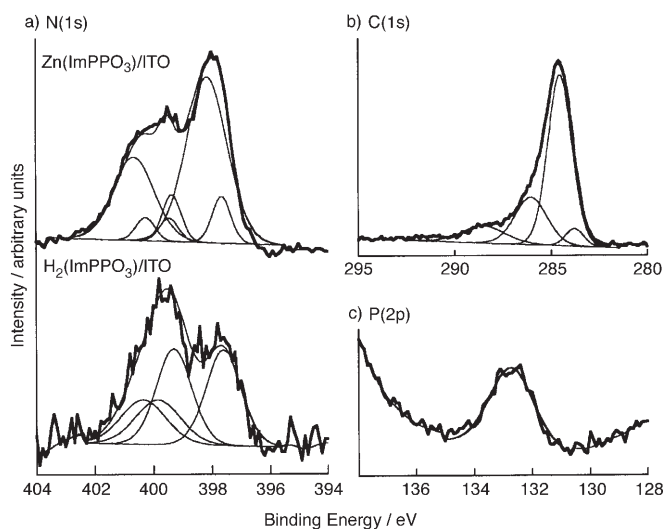

Figure 5. XPS deconvoluted profiles before and after zinc incorporation into H₂(ImPPO₃) on an ITO surface in the N(1s) region (a). XPS spectra of Zn(ImPPO₃)/ITO in the C(1s) region (b) and the P(2p) region (c).

assemblies. For the monolayer assemblies on the ITO electrode, the Soret band was found to show a bathochromic shift, suggesting that the porphyrin planes are in a mutually tilted orientation. Organization of the SP-mimic structure resulted in a slight broadening of the Soret band, even though 40% of the porphyrin afforded the SP-mimic dimer as described below. Similar spectral changes in the course of the organization/metathesis processes were observed for each porphyrin anchor. Therefore, the organized structures are identical, irrespective of the anchoring group, even though the surface concentrations vary considerably.

XPS measurements were adopted for further structural elucidation of Zn(ImPPh)/Zn(ImPPO₃)/ITO. After H₂-(ImPPO₃) monolayer formation, the O(1s) peak at 531.8 eV decreased drastically (Figure 2b). In the P(2p) region, observation of a unimodal peak indicates that the phosphonate group exists as a single chemical species (Figure 5c). The phosphonate group is assumed to react with the surface terminal OH groups in linking to the ITO surface. H₂(ImPPO₃)

monolayer assembly showed characteristic peaks of the free-base porphyrin at 397.6 and 399.3 eV in the N(1s) region (Figure 5a).[31] The split N(1s) peaks were unified to a single peak at 398.1 eV by the introduction of zinc due to structural equivalence.[32] From peak deconvolution for the N(1s) region, zinc atoms were estimated to be inserted into 80% of the porphyrin centers on the ITO surface. The peak of the nitrogen of the imidazolyl residue is somewhat unclear, since the N(1s) peak may involve shake-up satellite in the higher binding energy region. In the C(1s) region, the characteristic peaks attributable to C=C and C−N bonding appeared at 286.0 and 288.5 eV, respectively, in addition to that of the residual carbon at 284.4 eV (Figure 5b).[33] The Zn(2p) peak was not available for the estimation of zinc insertion, because immersion of the ITO electrode in a solution of zinc acetate led to adsorption of excess zinc ions on its surface, judging from the large Zn(2p) peak.[32] The ratio of P(2p) to N(1s) indicates that the SP-mimic dimer was formed by organization/metathesis of Zn(ImPPh) on 50% of the Zn(ImPPO₃) layer. Consequently, H₂(ImPPO₃) (20%), Zn(ImPPO₃) in a tilted orientation (40%), and Zn-(ImPPh)/Zn(ImPPO₃) as the SP-mimic structure (40%) were immobilized on the sol–gel-modified ITO surface.

Anodic photocurrent generation

Effect of the SP-mimic dimer structure: The SP-mimic modified ITO was mounted at a round cell window (6 mm diameter) and exposed to a buffered aqueous solution containing 1.0 M NaClO₄ as electrolyte and 50 mM hydroquinone (H₂Q) as a sacrificial electron donor. Steep rise and depletion were observed as soon as the light irradiation was turned on and off, respectively. Typical photoresponse patterns are shown in Figure 6. The magnitude of the anodic photocurrent showed a dependence on the applied potential and the excitation wavelength. Prompt photoresponse persisted over at least several hours during the experimental operations.

Figure 7 depicts the photocurrent action spectra and their corresponding absorption spectra on the ITO electrode. The maximum photocurrent at each ITO electrode was obtained by excitation at 400–410 nm. Close similarity between the
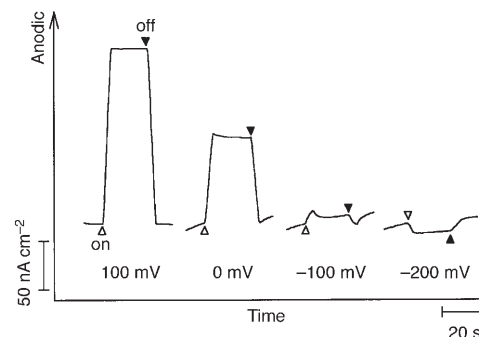

Figure 6. Photocurrent response of Zn(ImPPh)/Zn(ImPPO₃)/ITO excited at 410 nm (intensity: 98.2 μW cm⁻²) under biased conditions at 100, 0, −100, and −200 mV versus Ag/AgCl (left to right) (pH 6.2).

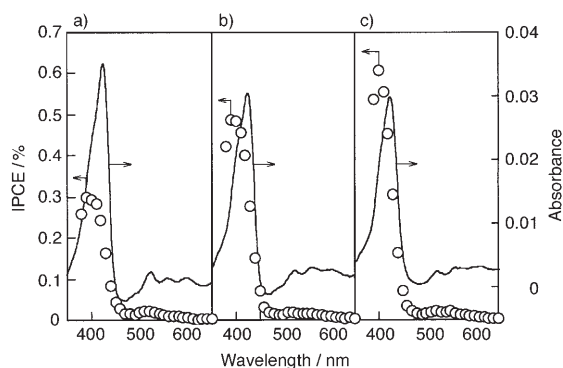Figure 7. Photocurrent action spectra of $H_2(ImPPO_3)$/ITO (a), Zn-$(ImPPO_3)$/ITO (b), and Zn(ImPPh)/Zn$(ImPPO_3)$/ITO (c) in the presence of 50 mM hydroquinone in aqueous solution with 1.0 M NaClO$_4$ as supporting electrolyte (pH 6.2) at 100 mV versus Ag/AgCl.
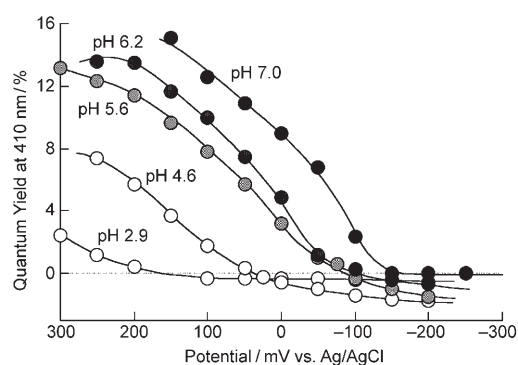

Figure 8. Potential dependence of the anodic photocurrent of Zn-(ImPPh)/Zn$(ImPPO_3)$/ITO excited at 410 nm at various pH values.

action spectra and the corresponding absorption spectra proves that the observed photocurrent was attributable to photoexcitation of the surface-confined porphyrin. Zinc incorporation and dimer formation enhanced the anodic photocurrent. Simple comparison can be made on the basis of the photocurrent quantum yield, Φ, which excludes the difference of the absorbances of the ITO surfaces.

Comparison of the photocurrent action spectra helps to elucidate the charge-injection mechanisms (Figure 7 and Table 1). Relatively low and similar quantum yields for anodic photocurrent generation from both the S_1^* and S_2^* states for $H_2(ImPO_3)$/ITO are suggestive of low charge-injection efficiency and/or high charge recombination. In a

Table 1. Quantum yield and IPCE (incident photon-to-current efficiency) for the anodic photocurrent obtained by excitation at 410 nm (Soret band) and 550 nm (Q band) in aqueous electrolyte containing H_2Q (50 mM) at 100 mV versus Ag/AgCl (pH 6.2).

	Φ_{410}/Φ_{550} [%]	IPCE$_{410}$/IPCE$_{550}$ [%]
$H_2(ImPPO_3)$/ITO	4.7/3.8	0.28/0.01
Zn$(ImPPO_3)$/ITO	8.2/2.3	0.46/0.015
Zn(ImPPh)/Zn$(ImPPO_3)$/ITO	10.0/4.3	0.55/0.03
Zn(ImPPh)/Zn$(ImPAc_2)$/ITO	4.8/2.9	0.16/0.005
Zn(ImPPh)/Zn$(ImPS_2)$/ITO	0.9/0.02	0.02/0.0006

similar manner, photoexcitation at the Q band (S_1) of Zn-$(ImPPO_3)$/ITO and Zn(ImPPh)/Zn$(ImPPO_3)$/ITO is less effective for anodic photocurrent generation ($\Phi_{550} = 2.3$–4.3%) compared with excitation at the Soret band ($\Phi_{410} = 8.2$–10.0%) at 100 mV. Combining these observations, it is assumed that the photo-liberated electron hardly exceeds the activation barrier for charge injection from the H_2–porphyrin or the S_1^* state of the Zn–porphyrin. In contrast, the higher potential of the S_2^* state is appropriate for charge injection. This enhancement may stem from the shift of the redox potentials. Furthermore, the SP-mimic dimer formation augments the anodic photocurrent, even though the absorption stays at a similar level, whereby Φ_{410} is improved from 8.2% to 10%. The enhanced photocurrent generation proves the advantage of the slipped-cofacial dimer in providing photoinduced charge separation.

The potential diagram depicts the mechanism of the anodic photocurrent generation (Scheme 3). It is known that the conduction band (CB) for an ITO electrode is located at
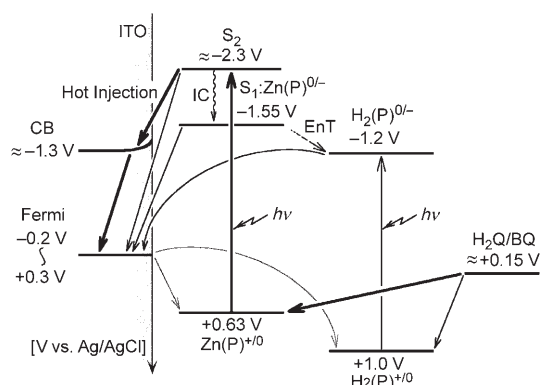
Scheme 3. Potential diagram for anodic photocurrent generation of Zn-(ImPPh)/Zn(ImPR)/ITO by excitation at the Soret band in aqueous hydroquinone (50 mM). Potentials are estimated based on refs. [14, 34] and absorption spectra. The S_2 state of $H_2(ImPPO_3)$ at -1.9 V is omitted for the sake of clarity.

around -1.3 V versus Ag/AgCl.[10c] This value is consistent with the reduction potential of the ITO electrode itself, which is the negative limit of the potential window. In CH_2Cl_2, the H_2–porphyrin, the SP-mimic dimer, and the dissociated monomer of the Zn–porphyrin are reduced at -1.2, -1.55, and -1.54 V versus Ag/AgCl, respectively.[34] Therefore, the S_1 levels of the H_2– and Zn–porphyrins are not sufficient for electron transfer to the CB level. In contrast, the S_2 level of the Zn–porphyrin at -2.3 V is considerably higher and exceeds the driving force for electron transfer to the CB level. However, the S_2 level of the H_2–porphyrin at -1.9 V may be less effective in generating an anodic photocurrent, considering that similar quantum yields are observed for photoexcitation at the Soret and Q-band regions. The high anodic photocurrent efficiency observed upon photoexcitation at the Soret band of the Zn–porphyrin may be attributed to hot injection from the S_2 level directly into the CB before internal conversion (IC) to the S_1 level. On the

other hand, the photocurrent from S_1^* states involves charge injection into the Fermi level. The charge separation in the S_2^* state points to strong coupling[35] between the band levels of the porphyrin and ITO. Direct anchoring on the ITO surface via a phosphonate group without any insulating bonds is thus concluded to be satisfactory for strong coupling between the S_2^* state and the CB level. For instance, no steady-state fluorescence was detectable, supporting this conclusion.

The slipped-cofacial porphyrin dimer, which accelerates charge separation and retards charge recombination,[21] is considered to contribute to efficient sequential electron transfer across the junction Zn(ImPPh)/Zn(ImPPO₃)/ITO in the presence of H₂Q. The H₂(ImPPO₃) site, coexisting with Zn(ImPPh)/Zn(ImPPO₃), may trap excitation energy as an energy sink.[36] On the other hand, the monomer site of Zn-(ImPPO₃) possesses almost similar HOMO–LUMO levels to those of Zn(ImPPh)/Zn(ImPPO₃). The enhanced anodic photocurrent from the S_2^* state of photoexcited Zn-(ImPPh)/Zn(ImPPO₃) as the SP-mimic points to effective electron transfer to the CB level. Therefore, the lateral energy-transfer (EnT) process may be negligible in Zn-(ImPPh)/Zn(ImPPO₃)/ITO. Hot electron injection from the S_2 photoexcited Zn–porphyrin into the ITO levels with very high quantum yield is the dominant process in the anodic photocurrent generation.

The enlarged ionic radius of the porphyrin dimer is effective in providing a long-lived charge-separated state.[21] The anodic photocurrent may be enhanced by the effect of the cofacial dimer together with the effect of organized water molecules in the vicinity of the ITO surface, assuming that backward electron transfer in the aqueous solution occurs in the deep "inverted" regime of the Marcus parabola. Besides, the aqueous environment may affect the ITO surface, because to some extent the ITO surface remains "naked" after immobilization of the SP-mimic porphyrin dimers on the surface (see the blocking experiments in the Supporting Information). The Gouy–Chapman–Stern model proposes that hydrating water molecules in the vicinity of the metal oxide electrode surface constitute a Helmholtz layer. This is supported by the observation of distinct effects of structured water or water clusters in facilitating electron transfer at metal oxide/water interfaces on the sub-femtosecond time-scale, the so-called "wet-electron" states.[37,38] This assumption may account for more effective sensitization at the Soret band than that in the Q-band region in the photocurrent action spectra. Therefore, the S_2 photoexcited singlet state facilitates efficient charge injection directly into the conduction band. Such an effect may be relevant to the improvement of anodic photocurrent through modification of the pH conditions as discussed below.

Potential variation: The anodic photocurrent quantum yield (Φ_{410}) of the Zn(ImPPh)/Zn(ImPPO₃)/ITO system increased on applying more anodic potentials and saturated at around 13–15% at +100–200 mV versus Ag/AgCl, which is close to the oxidation potential of H₂Q in the bulk (Figure 8). The

photocurrent is therefore limited by the redox process of the H₂Q sacrificial electron donor. These Φ_{410} values are comparable to the values of 11–19.5% obtained for a porphyrin–fullerene dyad system on ITO electrodes.[9] Therefore, the above values are surprisingly high considering the fact that no redox cascade structure incorporating electron donors or acceptors is employed.

On applying more anodic potentials, the anodic photocurrent increased. The concomitant shift of the CB level with the Fermi level results in band bending, even though the band-edge potential remains at the same level under certain pH conditions (Scheme 1a–c). Therefore, a large anodic potential can bend the CB structure to form a Schottky barrier to suppress the backward electron-transfer process from the CB to the vacant S_0 level. On the other hand, the Fermi level, without a band structure, is not effective for such a unidirectional electron transfer. The phosphonate anchor, promoting the hot injection from the S_2^* state to the CB, may modify the CB structure at the ITO surface.

pH variation and anchoring group effect: Variation of the pH revealed the important influence on the surface state of the ITO electrode in manipulating the surface dipole and the band-edge potential. The pH effects of isophthalate and thiolate anchoring groups on the photocurrent properties were compared with that of the phosphonate anchor (Figures 9 and 10). Although the anodic photocurrent of the Zn-(ImPPh)/Zn(ImPPO₃)/ITO system was improved dramati-

Figure 9. Potential dependence of the anodic photocurrent of Zn-(ImPPh)/Zn(ImPAc₂)/ITO excited at 410 nm in the presence of 50 mM hydroquinone with 1.0 M NaClO₄ as supporting electrolyte at various pH values.

cally on increasing the pH, the photocurrents of the Zn-(ImPPh)/Zn(ImPAc₂)/ITO and Zn(ImPPh)/Zn(ImPS₂)/ITO systems showed only a small improvement on varying the pH. Fromherz and Arden have established the pH dependence of V_{fb}.[13] Depending on the pH, the surface states of n-type semiconductor electrodes are strongly affected by the potential drop across the bulk medium in the Helmholtz layer.[13,39] Comparison of the pH dependences for the anchoring groups implies that the surface state strongly depends on the surface anchoring group.
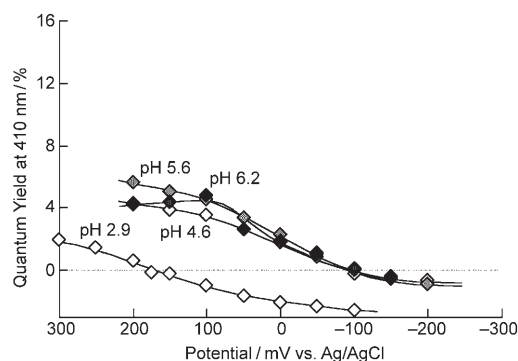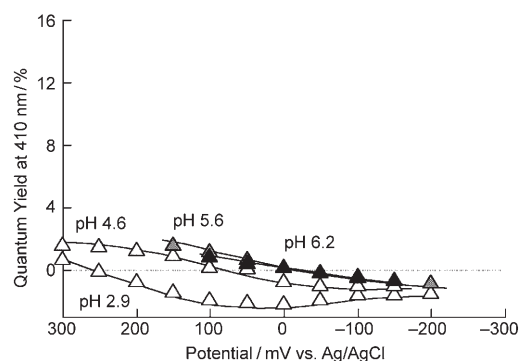
Figure 10. Potential dependence of the anodic photocurrent of Zn-(ImPPh)/Zn(ImPS$_2$)/ITO excited at 410 nm in the presence of 50 mm hydroquinone with 1.0 m NaClO$_4$ as supporting electrolyte at various pH values.

The apparent V_{fb} for the porphyrin-modified ITO was evaluated from the zero-current intercept in the I–V plots (Figures 8, 9, and 10). Apparent V_{fb} is plotted as a function of pH in Figure 11. At alkaline pH, the apparent V_{fb} is shifted to more cathodic potentials. As the pH increases, the
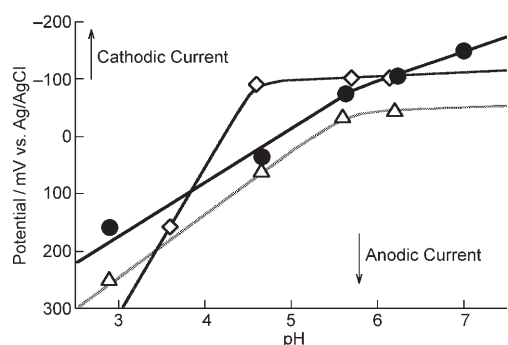

Figure 11. Plot of the apparent flat-band potential (V_{fb}) as a function of pH conditions for Zn(ImPPh)/Zn(ImPR)/ITO (R = −PO$_3$ (●), -Ac$_2$ (♦), and -S$_2$ (△)).

band-edge potentials are therefore assumed to rise and provide higher Schottky barriers, suppressing backward electron transfer from the CB to the porphyrin radical cation (Scheme 1a–c). Since the slope in the V_{fb}–pH plot exceeds the Nernstian slope of H$_2$Q (-59 mV (pH)$^{-1}$),[40] the efficiency of anodic photocurrent generation is determined not only by the redox potential of H$_2$Q, but also by the ITO surface state. The V_{fb} value of intrinsic n-type semiconductors normally changes linearly as a function of pH.[39] Thus, a relatively linear pH dependence of V_{fb} for Zn(ImPPh)/Zn-(ImPPO$_3$)/ITO supports the assumption that the conduction band of the ITO electrode and porphyrin are strongly coupled via the phosphonate group (Figure 11). On the other hand, the existence of inflection points may be attributed to a protonation–deprotonation equilibrium of the physisorbed species. This may imply that the surface charge of ITO affects the band-edge potentials.[41] However, the detailed

mechanism underpinning this phenomenon requires further study.

The apparent V_{fb} value could be tuned by varying the anchoring porphyrin. The apparent V_{fb} values for Zn(ImPPh)/Zn(ImPS$_2$)/ITO were more anodic than those for Zn-(ImPPh)/Zn(ImPPO$_3$)/ITO and Zn(ImPPh)/Zn(ImPAc$_2$)/ITO. As a consequence, larger anodic potentials must be applied to generate an anodic photocurrent in the Zn(ImPPh)/Zn(ImPS$_2$)/ITO system. The higher Schottky barrier, created by surface modification with phosphonate and isophthalate groups, is therefore advantageous for anodic photocurrent generation. With the aim of fabricating dye-sensitized solar cells, this anchoring group effect has been verified on a TiO$_2$ surface, although the results are not yet conclusive.[42,43] The present study has demonstrated that a Zn(ImPPO$_3$)-based SP-mimic can modify the band-edge potential, and so enhances the n-type semiconductor characteristics of the ITO electrode. This allows an efficient conversion of the photoexcited state and leads to increased electric current generation. Phosphonate-modified ITO thus promotes hot injection to afford a larger Φ_{410} for the anodic photocurrent at 100 mV versus Ag/AgCl (pH 6.2) by a factor of two and by a factor of ten compared with those of isophthalate-modified and thiolate-modified ITO, respectively (Figure 12, and
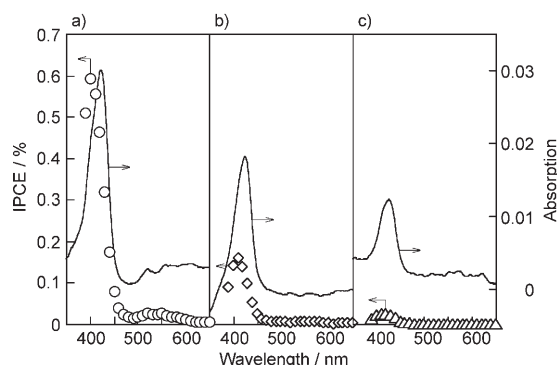
Figure 12. Photocurrent action spectra of Zn(ImPPh)/Zn(ImPPO$_3$)/ITO (a), Zn(ImPPh)/Zn(ImPAc$_2$)/ITO (b), and Zn(ImPPh)/Zn(ImPS$_2$)/ITO (c) in the presence of 50 mm hydroquinone in aqueous solution containing 1.0 m NaClO$_4$ as supporting electrolyte (pH 6.2) at 100 mV versus Ag/AgCl.

Figure S6 in the Supporting Information). The effect of the different anchoring groups on the efficiency of the photocurrent generation should be related to the nature of the chemical linkage and the surface state, and therefore to the charge-injection step. The rate-determining step is therefore electron injection into the ITO anode, that is, the hot-injection process from the S$_2$ photoexcited state.

Unusual concentration effect: It is important to note that measurements of Soret band absorbance on ITO indicated that Zn(ImPPO$_3$) has a higher surface concentration than Zn(ImPAc$_2$) or Zn(ImPS$_2$). Figure 12 represents the photocurrent action spectra and their corresponding absorption

Figure 13. Experimental setup for photocurrent generation.[10c]

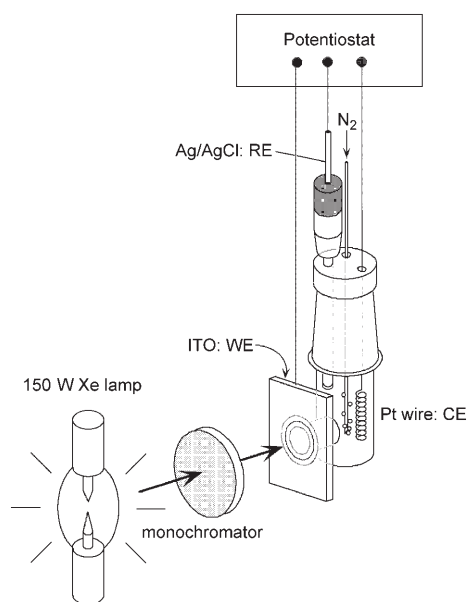spectra of the SP-mimic on the ITO electrode. This comparison clearly shows the difference in the efficiencies of photocurrent generation (Table 1). It is generally observed that Φ values increase on dilution of the porphyrin surface concentration in conventional monolayer assemblies.[44] This is probably due to the decrease in the number of deactivation pathways.[44] However, the SP-mimic porphyrin assemblies are ordered in a slipped-cofacial orientation and these systems appear to be insensitive to such processes, even when the surface concentration is increased. Phosphonate-modified ITO serves as a good electron acceptor and so should enhance the effect of the SP-mimic dimer in the charge-separation step, and this should in turn lead to amplification of the anodic photocurrent from the S_2 photoexcited state. As a consequence of its high surface concentration and exceptionally high efficiency, the photoexcitation of Zn(ImPPh)/Zn(ImPPO$_3$)/ITO generates remarkably large photocurrents.

Conclusion

A novel surface fabrication approach utilizing a surface sol–gel process and molecular organization has been performed with the aim of obtaining efficient photoexcited charge injection. The nucleophilicity of the terminal OH groups of ITO has been successfully improved by sol–gel modification with Ti(OnBu)$_4$, such that monolayer assemblies could be readily immobilized with appropriate anchoring groups.

Exploration of the photocurrent properties has allowed elucidation of the role of the conduction band in the photoexcited charge-injection process. The increase in band-edge potential due to the introduction of Zn(ImPPO$_3$) led to an increase in the anodic photocurrent to 15% at Φ_{410}. This was achieved even without incorporating a redox gradient

on the flat ITO electrode. The effect of pH suggests that the surface state of the ITO is dependent on the anchoring species. Thus, the anchoring species has an impact on the magnitude of the anodic photocurrent.

We consider that the high efficiency observed for photocurrent generation may stem not only from the phosphonate-modulated ITO surface, but also from the increased radius of the radical cation.[21] The especially high quantum yield for the anodic photocurrent from the S_2^* state compared with that from the S_1^* state would suggest that sufficiently fast charge injection occurs before internal conversion to the S_1^* state. Comparison of the photocurrent action spectra supports the view that the difference in driving forces from the S_2^* and S_1^* states to the ITO conduction band level is critical for the anodic photocurrent generation. We assume that the effect of the cofacial dimer is enhanced in aqueous media, providing a deep "inverted" Marcus regime for the SP-mimic dimer and a "wet-electron" effect to stabilize the liberated electron on the sol–gel-treated ITO surface.

The phenylphosphonyl group is especially effective in facilitating strong electronic communication between the S_2^* state of the Zn–porphyrin and the ITO conduction band, as evidenced by XPS observation, the photocurrent action spectra, and the pH variation of the apparent flat-band potentials. The Zn(ImPPO$_3$)/ITO scaffold can provide facile immobilization of multiporphyrin arrays for extensive photovoltaic applications.[22] The present insights are important for understanding the essential principle underlying interfacial electron transfer at the ITO electrode. This approach allows the rational design of molecule/ITO junctions for further elaborate self-assembling systems. An artificial photosynthetic reaction center based on the "special pair"-mimic structure on the ITO electrode is currently under construction with a view to achieving more efficient anodic photocurrent generation based on redox cascade alignment for sequential electron transfer.

Experimental Section

General: ^{1}H NMR spectra were recorded on JEOL JNMEX 270 (270 MHz) or JEOL ECP 600 (600 MHz) spectrometers; chemical shifts are referenced to TMS as an internal standard. ^{31}P NMR spectra were acquired under off-spinning conditions and are referenced to 85% aqueous phosphoric acid inside a sealed capillary as an external standard. The procedure for the synthesis of Zn(ImPPh) has been described elsewhere.[45]

Diethyl 4-formylbenzphosphonate (1): A solution of 4-bromobenzaldehyde (1.5 g, 8 mmol) in toluene (3 mL) was concentrated to two-thirds of its original volume for the azeotropic removal of water. Diethyl phosphite (1.2 g, 1.1 equiv) and triethylamine (1.2 mL) were then added. The mixture was transferred to a Schlenk flask, degassed by repeated freeze–pump–thaw cycles, and purged with argon. Tetrakis(triphenylphosphine)-palladium(0) (600 mg) was then added and the mixture was stirred at 90°C for 7 h.[46] In the course of the coupling reaction, the reaction mixture changed from brown to pale greenish-brown. Diethyl ether was then added to the reaction mixture and the precipitate that formed was filtered off. Diethyl 4-formylbenzphosphonate was purified by Kugelrohr distillation and was obtained as a slightly yellowish liquid. The coupling

reaction was successfully accomplished without any protection of the aldehyde residue, giving the product in a fair yield (0.79 g, 41%). ^{1}H NMR (270 MHz, CDCl$_3$): δ = 1.34 (t, J = 7.0 Hz, 6H; POCH$_2$CH$_3$), 4.07–4.24 (m, 4H; POCH$_2$CH$_3$), 7.96–8.00 (m, 4H; Ph), 10.09 ppm (s, 1H; -CHO); ^{31}P NMR (242 MHz, CDCl$_3$): δ = 16.89 ppm.

5-(1-Methylimidazol-2-yl)-10,20-bis(3-allyloxypropyl)-15-(4-diethoxyphosphonylphenyl)porphyrin (2): 2-Formyl-1-methylimidazole (0.18 g, 1 equiv), aldehyde **1** (0.41 g, 1 equiv), and meso-(3-allyloxypropyl)dipyrromethane (0.82 g, 2 equiv) were dissolved in CHCl$_3$ (850 mL) and stirred at room temperature in the presence of trifluoroacetic acid (TFA) (3 equiv) for 3 h. Chloranil (4 equiv) and triethylamine (1 equiv) were then added to the reaction mixture to oxidize the porphyrinogen intermediate, and the mixture was stirred overnight. The crude mixture was subjected to column chromatography on silica gel (eluents: CHCl$_3$ and CHCl$_3$/acetone, 2:1, v/v) three times. The desired porphyrin **2** was isolated as a purple solid (86 mg, 6%). ^{1}H NMR (270 MHz, CDCl$_3$): δ = −2.69 (s, 2H; inner pyrrole), 1.34 (t, J = 5.0 Hz, 6H; POCH$_2$CH$_3$), 2.78 (t, J = 5.0 Hz, 4H; -CH$_2$CH$_2$O-allyl), 3.39 (s, 3H; imidazolyl-CH$_3$), 3.65 (t, J = 5.0 Hz, 4H; -CH$_2$O-allyl), 4.07 (t, J = 5.0 Hz, 4H; -CH$_2$(CH$_2$)$_2$O-allyl), 4.38–4.44 (m, 4H; POCH$_2$CH$_3$), 5.13 (t, J = 7.2 Hz, 4H; -OCH$_2$CH=CH$_2$), 5.26 (dd, J = 13.5, 1.9 Hz, 2H; -CH$_2$CH=CHH), 5.26 (dd, J = 17.6, 1.9 Hz, 2H; -CH$_2$CH=CHH), 6.02–6.07 (m, 2H; -OCH$_2$CH=CH$_2$), 7.47 (d, J = 1.4 Hz, 1H; 5-imidazolyl), 7.68 (d, J = 1.4 Hz, 1H; 4-imidazolyl), 8.1–8.4 (m, 4H; Ph), 8.80 (d, J = 4.9 Hz, 4H; β-pyrrole), 9.52 ppm (dd, J = 11.1, 5.1 Hz, 4H; β-pyrrole); MALDI-TOF MS: m/z calcd for **2**: 798.37; found: 799.54.

H$_2$(ImPPO$_3$) (3): A flask charged with **2** (85 mg) and potassium bromide (1.7 g) was purged with argon. Dry triethylamine (2.8 mL) and dry DMF (16 mL) were then added, followed by chlorotrimethylsilane (TMSCl, 2.6 mL), and the mixture was stirred at 60–65°C for 24 h.[47] A white precipitate that formed in the course of the deprotection was filtered off. After evaporation of the solvent, the mixture was dispersed in water (60 mL) and concentrated HCl (0.5 mL) and stirred at room temperature for 3 h. The aqueous phase was neutralized with sodium hydrogencarbonate, the desired porphyrin was extracted with CHCl$_3$, and the combined extracts were dried over anhydrous sodium sulfate. The porphyrin was extracted with MeOH and purified by reprecipitation from diethyl ether. The desired porphyrin was obtained almost quantitatively. ^{1}H NMR (270 MHz, CD$_3$OD): δ = 2.59 (t, J = 6.5 Hz, 4H; -CH$_2$CH$_2$O-allyl), 3.41 (s, 3H; imidazolyl-CH$_3$), 3.58 (t, J = 5.7 Hz, 4H; -CH$_2$CH$_2$O-allyl), 3.96 (d, J = 5.7 Hz, 4H; -OCH$_2$CH=CH$_2$), 4.91 (t, J = 7.3 Hz, 4H; -CH$_2$(CH$_2$)$_2$O-allyl), 5.11 (d, J = 12.2 Hz, 2H; -CH$_2$CH=CHH), 5.27 (dd, J = 15.4 Hz, 2H; -CH$_2$CH=CHH), 5.89–5.95 (m, 2H; -OCH$_2$CH=CH$_2$), 7.56 (s, 1H; 5-imidazolyl), 7.67 (d, J = 0.8 Hz, 1H; 4-imidazolyl), 8.07–8.14 (m, 4H; Ph), 8.10 (d, J = 30.5 Hz, 4H; β-pyrrole), 9.49 ppm (d, J = 30.5 Hz, 4H; β-pyrrole); MALDI-TOF MS: m/z calcd for **3**: 742.30; found: 742.26.

3,5-Diethoxycarbonylbenzaldehyde (4): Diethyl 5-(hydroxymethyl)isophthalate was obtained from benzene-1,3,5-triethoxycarbonate by reduction with LiBH$_4$ in dry THF. Subsequent oxidation of 3,5-triethoxycarbonylbenzyl alcohol with PCC (pyridinium chlorochromate) in dry chloroform afforded 3,5-diethoxycarbonylbenzaldehyde. In the literature procedure,[48] oxidation to the aldehyde was achieved with CAN (cerium(IV) ammonium nitrate) as the oxidant. In our trial, we found it difficult to prevent over-oxidation to the corresponding carboxylic acid with CAN. Instead, oxidation with PCC was found to smoothly afford the desired product (94%).

The synthesis of 4-{5-(1-methylimidazol-2-yl)-10,20-bis(3-allyloxypropyl)-porphyrin-15-yl}benzphosphonic acid, H$_2$(ImPPO$_3$) (**3**), is shown in Scheme 4.
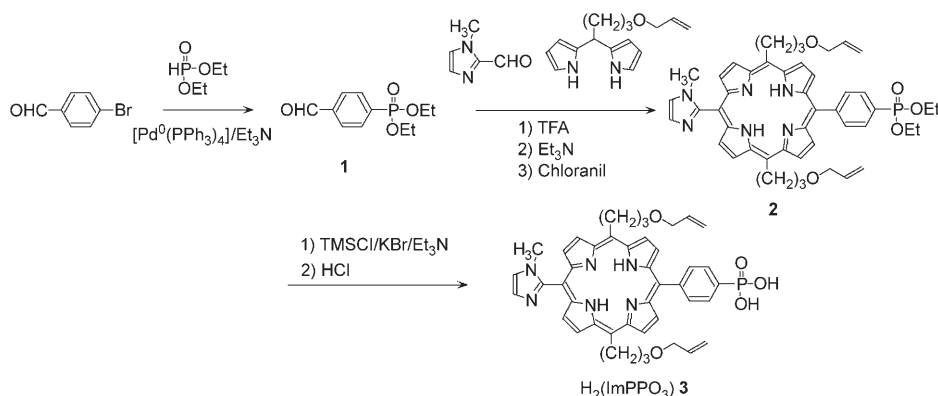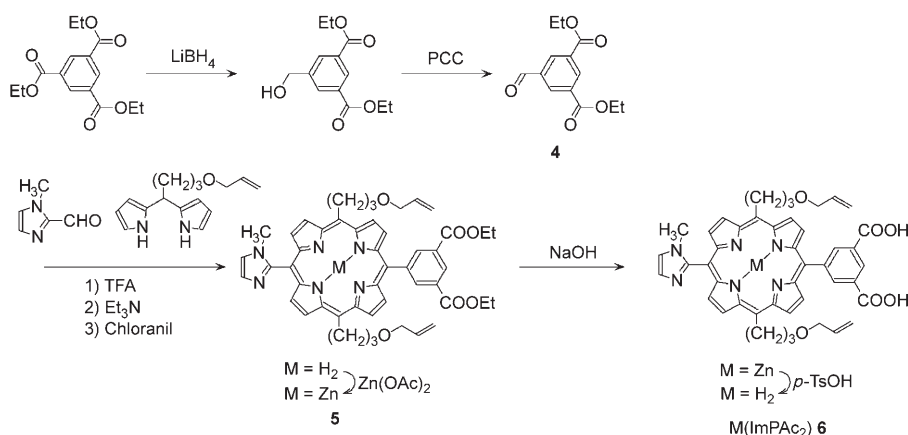

Scheme 4. Synthesis of H$_2$(ImPPO$_3$) (**3**).

5-(1-Methylimidazolyl)-10,20-bis(3-allyloxypropyl)-15-(3,5-diethoxycarbonylphenyl)porphyrinatozinc (5): Porphyrin **5** was synthesized by TFA-catalyzed cyclization. TFA (3 equiv) was added to a mixture of 2-formyl-1-methylimidazole (0.18 g, 1 equiv), **4** (0.42 g, 1 equiv), and meso-(3-allyloxypropyl)dipyrromethane (0.82 g, 2 equiv) in CHCl$_3$ (850 mL). The reaction mixture was stirred at room temperature for 4 h, chloranil (4 equiv) was added, and stirring was continued for a further 10 h. The reaction mixture was then neutralized by washing with saturated aqueous sodium hydrogencarbonate solution and brine. The crude free-base porphyrin was obtained by using column chromatography on silica gel eluting with CHCl$_3$/acetone (9:1, v/v) (yield 133 mg, 9%). The crude porphyrin was metalated by treating it with an aliquot of a saturated solution of zinc acetate in MeOH (3 mL). The title zinc porphyrin **5** was obtained by using column chromatography on silica gel, eluting with CHCl$_3$/acetone (9:1, v/v). ^{1}H NMR (270 MHz, CDCl$_3$): δ = 1.38 (t, J = 7.0 Hz, 3H; -COOCH$_2$CH$_3$), 1.63 (t, J = 7.0 Hz, 3H; -COOCH$_2$CH$_3$), 1.69 (s, 3H; imidazolyl-CH$_3$), 2.14 (d, J = 1.6 Hz, 1H; 4-imidazolyl), 3.09 (m, 4H; -CH$_2$CH$_2$O-allyl), 3.94 (t, J = 7.3 Hz, 4H; -CH$_2$(CH$_2$)$_2$O-allyl), 4.24 (d, J = 5.4 Hz, 4H; -OCH$_2$CH=CH$_2$), 4.48, 4.68 (q, J = 7.0 Hz, 4H; -COOCH$_2$CH$_3$), 5.25 (t, J = 7.3 Hz, 4H; -CH$_2$(CH$_2$)$_2$O-allyl), 5.34 (d, J = 10.3 Hz, 2H; -CH$_2$CH=CHH), 5.44 (d, J = 4.86 Hz, 2H; -CH$_2$CH=CHH), 5.44 (d, J = 10.5 Hz, 2H; -OCH$_2$CH=CHH), 5.45 (s, 1H; 5-imidazolyl), 5.55 (d, J = 1.6 Hz, 2H; β-pyrrole), 6.13–6.24 (m, 2H; -OCH$_2$CH=CH$_2$), 8.89 (d, J = 1.6 Hz, 2H; β-pyrrole), 8.94 (s, 1H; 4-Ph), 8.98 (d, J = 4.6 Hz, 2H; β-pyrrole), 9.21, 9.54 (s, 2H; 2,6-Ph), 9.66 ppm (d, J = 4.6 Hz, 2H; β-pyrrole); MALDI-TOF MS: m/z calcd for **5**: 868.29; found: 867.996.

H$_2$(ImPAc$_2$) (6): Diethyl Zn–porphyrinyl isophthalate **5** (100 mg) was dissolved in THF/ethanol (13:7, v/v) at room temperature and stirred in the presence of 8N NaOH for 3 h. The crude mixture was then washed with brine and extracted with chloroform. The organic layer was treated with p-toluenesulfonic acid monohydrate (p-TsOH) to displace the central zinc. The bright-blue organic layer was washed with a large excess of brine, which resulted in a color change to red due to neutralization, and dried over anhydrous sodium sulfate. The desired porphyrin was obtained as a brownish-red solid (35%). ^{1}H NMR (270 MHz, [D$_6$]DMSO, 60°C): δ = −2.76 (s, 2H; inner pyrrole), 2.08 (s, 3H; imidazolyl-CH$_3$), 3.5 (br, 4H; -CH$_2$CH$_2$O-allyl), 4.0 (br, 4H; -CH$_2$(CH$_2$)$_2$O-allyl), 4.2 (br, 4H; -OCH$_2$CH=CH$_2$), 4.8 (br, 4H; -COOCH$_2$CH$_3$), 5.2 (br, 4H; -CH$_2$(CH$_2$)$_2$O-allyl), 5.3 (br, 2H; -CH$_2$CH=CHH), 6.5 (br, 2H; -CH$_2$CH=CHH), 7.54 (s, 1H; 4-imidazolyl), 7.77 (s, J = 1.6 Hz, 1H; 5-imidazolyl), 8.68 (br, 3H; Ph), 8.8 (br, 4H; β-pyrrole), 9.6 ppm (br, 4H; β-pyrrole); MALDI-TOF MS: m/z calcd for **6**: 750.32; found: 752.592.

The synthesis of 5-{5-(1-Methylimidazolyl)-10,20-bis(3-allyloxypropyl)-porphyrin-15-yl}isophthalic acid, H$_2$(ImPAc$_2$) (**6**), is shown in Scheme 5.

Scheme 5. Synthesis of $H_2(ImPAc_2)$ (**6**).

Diethyl 5-(5,5-dimethyl-[1,3]dioxan-2-yl)isophthalate (7): A mixture of 3,5-diethoxycarbonylbenzaldehyde (**4**) (3.1 g, 12 mmol), 2,2-dimethyl-1,3-propanediol (1.6 g, 15 mmol), and *p*-TsOH (240 mg, 1.3 mmol) was refluxed in benzene (50 mL) in a two-necked flask equipped with a Dean–Stark trap and water condenser under an argon atmosphere. After refluxing at 100 °C for 4 h, the water that had collected in the Dean–Stark trap was separated. The mixture was washed with saturated aqueous sodium hydrogencarbonate and water, and the organic layer was dried over anhydrous sodium sulfate. The crude product was purified by using column chromatography on silica gel (eluent: hexane/ethyl acetate, 2:1, v/v) to furnish the title compound **7** as a white solid (yield 4.1 g, 98 %). ^1H NMR (270 MHz in CDCl$_3$): δ = 1.30 (s, 6H; CH$_3$-acetal), 1.41 (t, J = 7.3 Hz, 6H; CH$_3$-ester), 3.79 (dd, J = 35.37, 10.26 Hz, 4H; -CH$_2$), 4.42 (q, 4H; CH$_2$-ester), 5.41 (s, 1H; -CH), 8.36 (dd, J = 1.62, 0.54 Hz, 2H; Ph), 8.67 ppm (t, J = 1.62 Hz, 1H; Ph).

1-(5,5-Dimethyl-[1,3]dioxan-2-yl)-3,5-di(hydroxymethyl)benzene (8): A solution of diethyl 5-(5,5-dimethyl-[1,3]dioxan-2-yl)isophthalate (**7**) (4.0 g, 12 mmol) in dry diethyl ether (300 mL) was added dropwise to lithium aluminum hydride (0.90 g, 24 mmol) under a nitrogen atmosphere. The mixture was stirred at room temperature for 5 h, then cooled to 0 °C, and quenched by the addition of water (10 mL). It was then treated with 5 % sulfuric acid until a clear solution was obtained. The ethereal layer was separated and the aqueous layer was extracted with ethyl acetate (2 × 100 mL). The combined organic layers were washed with water (100 mL) and dried over anhydrous sodium sulfate. The crude material obtained was used for the next step without any further purification (yield 3.0 g, 99 %). ^1H NMR (270 MHz, CDCl$_3$): δ = 0.79 (s, 3H; -CH$_3$), 1.28 (s, 3H; CH$_3$), 2.79 (br, 2H; -OH), 3.73 (dd, J = 35.37, 10.26 Hz, 4H; -CH$_2$), 5.35 (s, 1H; -CH), 4.57 (s, 4H; CH$_2$-ester), 7.24 (s, 1H; Ph), 7.34 ppm (d, J = 0.54 Hz, 2H; Ph).

3,5-Di(bromomethyl)benzaldehyde (9): A solution of 1-(5,5-dimethyl-[1,3]dioxan-2-yl)-3,5-di(hydroxymethyl)benzene (**8**) (0.75 g, 3.0 mmol) in toluene (20 mL) was refluxed with 48 % aqueous HBr (18.8 mL) for 3.5 h. The reaction mixture was then diluted with water (20 mL). The organic layer was separated and the aqueous layer was extracted with ethyl acetate (2 × 100 mL). The combined organic layers were washed with 5 % aqueous sodium hydrogensulfite and water, and then dried over anhydrous sodium sulfate. The crude material was dissolved in chloroform (10 mL) and stirred with TFA (2.0 mL) and water (1.0 mL) for 20 h at room temperature. Aqueous sodium hydrogencarbonate (5 %, 50 mL) was added to the reaction mixture, and the organic phase was separated and dried over anhydrous sodium sulfate. The crude material was purified by using column chromatography on silica gel using *n*-hexane/ethyl acetate (4:1, v/v) as eluent to furnish the title compound **9**[49] as a light-yellow solid (yield 0.85 g, 98 %). TLC: R_f = 0.51 (hexane/ethyl acetate, 4:1, v/v); ^1H NMR (270 MHz, CDCl$_3$): δ = 4.53 (s, 4H; CH$_2$-ester), 7.70 (d, J = 1.89 Hz, 1H; Ph), 7.84 (d, J = 1.62 Hz, 2H; Ph), 10.01 ppm (s,

1H; C*H*O); ^{13}C NMR (67 MHz, CDCl$_3$): δ = 31.5, 129.7, 135.0, 137.2, 139.5, 190.7 ppm.

3,5-Di(acetylthiomethyl)benzaldehyde (10): A solution of 3,5-di(bromomethyl)benzaldehyde (**9**) (1.0 g, 3.4 mmol) and potassium thioacetate (0.94 g, 8.2 mmol, 2.4 equiv) in acetone (20 mL) was stirred at room temperature and then refluxed for 3 h. The reaction was then quenched by the addition of water (40 mL), and the mixture was extracted with ethyl acetate (2 × 100 mL). The combined organic layers were dried over anhydrous sodium sulfate. The crude mixture was purified by using column chromatography on silica gel using hexane/ethyl acetate (4:1, v/v) as eluent to furnish the title compound as a pale-yellow solid (yield 0.82 g, 85 %). TLC: R_f = 0.37 (hexane/EtOAc, 4:1, v/v); ^1H NMR (270 MHz, CDCl$_3$): δ = 2.37 (s, 6H; OAc), 4.14 (s, 4H; CH$_2$-ester), 7.49 (d, J = 1.62 Hz, 1H; Ph), 7.68 (d, J = 1.62 Hz, 2H; Ph), 9.96 ppm (s, 1H; CHO); ^{13}C NMR (67 MHz, CDCl$_3$): δ = 30.4, 32.7, 128.7, 135.0, 136.9, 139.3, 191.4, 194.3 ppm.

**H$_2$(ImPS$_2$) (11)**: A mixture of **10** (0.56 g, 2.0 mmol, 1.0 equiv), *meso*-(3-allyloxypropyl)dipyrromethane (0.98 g, 4.0 mmol, 2.0 equiv), and 2-formyl-1-methylimidazole (0.22 g, 1.0 mmol, 1.0 equiv) was dissolved in chloroform (400 mL). The mixture was degassed by bubbling nitrogen through it for 10 min and then TFA (0.15 mL, 2.0 mmol, 2.0 equiv) was added by means of a syringe over 30 s. The mixture was stirred at room temperature under a nitrogen atmosphere and then neutralized by adding triethylamine (1.1 mL, 2.0 mmol) and *p*-chloranil (0.74 g, 3.0 mmol) in THF (20 mL). The resulting mixture was then stirred at room temperature for 6 h. One-third of the solvent was removed in a rotary evaporator and the crude purple residue was chromatographed on silica gel using CHCl$_3$ as an eluent to yield the title compound **11** in almost 98 % purity. The compound was further chromatographed on silica gel using CHCl$_3$/acetone (10:1, v/v) as eluent. Finally, the material was passed through a column of basic alumina to afford the pure title porphyrin (yield 0.19 g, 12 %). TLC: R_f = 0.41 (CHCl$_3$/acetone, 10:1, v/v); ^1H NMR (270 MHz, CDCl$_3$): δ = -2.70 (s, 2H; inner pyrrole), 2.41 (s, 6H; -SCOCH$_3$), 2.792 (t, J = 6.5 Hz, 4H; -CH$_2$CH$_2$O-allyl), 3.41 (s, 3H; imidazolyl-CH$_3$), 3.66 (t, J = 5.7 Hz, 4H; -CH$_2$CH$_2$O-allyl), 4.08 (dd, J = 5.4, 1.4 Hz, 4H; -OCH$_2$CH= CH$_2$), 4.39 (d, J = 3.0 Hz, 4H; PhCH$_2$SAc), 5.11 (t, J = 7.3 Hz, 4H; -CH$_2$(CH$_2$)$_2$O-allyl), 5.26 (dd, J = 10.3, 1.4 Hz, 2H; -CH$_2$CH=CHH), 5.42 (dd, J = 15.7, 1.6 Hz, 2H; -CH$_2$CH=CHH), 6.03–6.14 (m, 2H; -OCH$_2$CH=CH$_2$), 7.47 (d, J = 0.8 Hz, 1H; 5-imidazolyl), 7.65 (s, 1H; 4-phenyl), 7.68 (d, J = 0.8 Hz, 1H; 4-imidazolyl), 7.93, 8.03 (s, 2H; 2,5-phenyl), 8.81 (dd, J = 10.0, 4.6 Hz, 4H; β-pyrrole), 9.52 ppm (dd, J = 15.1, 5.1 Hz, 4H; β-pyrrole); ^{13}C NMR (67 MHz, CDCl$_3$): δ = 29.75, 30.44, 31.36, 33.43, 34.52, 37.85, 69.14, 71.95, 104.31, 116.71, 119.29, 119.59, 121.23, 127.77, 128.20, 128.35, 129.10, 131.87, 133.73, 134.91, 136.11, 136.20, 143.00, 148.71, 194.64; MALDI-TOF MS: *m/z* calcd.: 839.08; found: 839.9; UV/Vis: λ_{max} (CH$_2$Cl$_2$) = 418, 516, 551, 592, 649 nm; fluorescence: λ_{em} (CHCl$_3$) = 654, 720 nm (λ_{ex} = 516 nm).

The synthesis of 5-(1-methylimidazol-2-yl)-10,20-bis(3-allyloxypropyl)-15-(3,5-diacetylthiomethylphenyl)porphyrin, $H_2(ImPS_2)$ (**11**), is shown in Scheme 6.

Procedures for ITO modification: The ITO substrate (commercially available from Geomatic Co., 2200 Å thick with a sheet resistance of 10 Ω per square) was cleaned by successive sonication in acetone, ethanol, and Milli-Q water. The metal species were estimated to be present in a ratio of 93.1 % In to 6.9 % Sn from XPS measurements (In:Sn $\approx$ 12:1). The surface chemical composition showed a good agreement with the analysis reported by Dunphy, Armstrong et al.[27b]

The ITO substrate was soaked in a solution of Ti(O*n*Bu)$_4$ (100 mM, purchased from Nacalai Tesque Co.) in toluene/ethanol (1:1, v/v) for
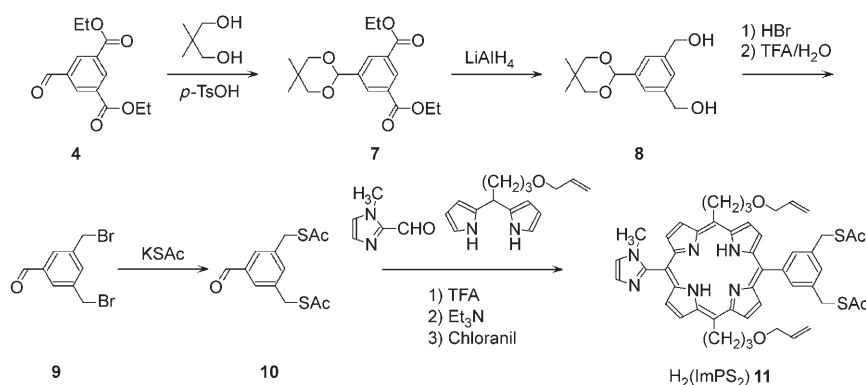
Scheme 6. Synthesis of H$_2$(ImPS$_2$) (**11**).

3 min.[24] It was then thoroughly rinsed with a large excess of ethanol and then with water to hydrolyze the *n*-butoxy groups on the surface. Prior to SAM formation, the ITO surface was cleaned by exposure to UV/ozone for 15 min.

The morphologies of the ITO surface before and after Ti(O*n*Bu)$_4$/hydrolysis treatment and subsequent hydrolysis were observed by means of noncontact atomic force microscopy (AFM, Seiko Instruments SPA 400) (Figure 1). The roughness factor was estimated to be 1.06 from the mean area per apparent area. This value is identical to that estimated before the titanium treatment, indicating that the titanium monolayer formation was not accompanied by undesirable domain formation and that the flatness of the surface of the ITO was maintained.

Zn(ImPAc$_2$) monolayer formation: The ITO glass was immersed in a 1.0 mм solution of H$_2$(ImPAc$_2$) in trifluoroethanol/dichloromethane (1:1, v/v) for 120 h. The central zinc was introduced by the same procedure as described for the Zn(ImPPO$_3$) monolayer. The Zn(ImPAc$_2$) monolayer on the titanium-treated ITO was shown to be robust during the immobilization procedures and photocurrent measurements. On the other hand, Zn(ImPAc$_2$) adsorbed on the bare ITO surface was completely cleaved in aqueous solution. For the conventional immobilization of carboxylates, DCC (dicyclohexylcarbodiimide as a condensing agent) condensation has been employed.[50] Successful covalent immobilization was thus achieved by the titanium treatment due to improved surface nucleophilicity.

Zn(ImPS$_2$) monolayer formation: The ITO glass was modified with thiol-functionalized imidazolyl–porphyrin as a monolayer assembly.[18b] Under Ar atmosphere at room temperature, the ITO surface was immersed for 20 h in a 0.1 mм solution of H$_2$(ImPS$_2$) in methanol containing 5 vol% of 28% NH$_4$OH.[51] Thioacetyl groups were cleaved by soaking in this alkaline solution, allowing attachment to the titanium-modified ITO surfaces. Strong absorbance at the Soret band was observed after rinsing with methanol and CH$_2$Cl$_2$.

Absorption spectra: Absorption spectra were measured by using a Shimadzu UV-3100PC spectrometer. Each spectrum was corrected for background absorption of the ITO electrode by subtraction.

Electrochemical and photocurrent measurements: The electrochemical investigation of the surface-confined porphyrin layers was carried out in an aqueous system under continuous nitrogen flow. The modified ITO working electrodes (WEs), mounted on 0.28 cm^2 of a round cell window, were exposed to aqueous buffered solution containing 1.0 м NaClO$_4$ as a supporting electrolyte. The pH conditions were adjusted by means of citric acid/Na$_2$HPO$_4$ buffer (pH 2.9–5.6) and phosphate buffer (Na$_2$HPO$_4$/ KH$_2$PO$_4$, pH 6.2–7.0). Platinum wire and Ag/AgCl(sat. KCl) were used as an auxiliary (CE) and a reference electrode (RE), respectively. The conventional three-electrode configuration was connected to a potentiostat (BAS, CV-50 W).

For anodic photocurrent generation, 50 mм hydroquinone (H$_2$Q), recrystallized from acetone, was dissolved in the buffered electrolyte solution as a sacrificial electron donor. The electrochemical cell was placed at a distance of 31 cm from the lamp house in the dark. The current was monitored under potentiostatic conditions during the on/off cycles of

light irradiation from a 150 W xenon arc lamp (Hamamatsu Photonics, L2274 light source equipped with a C7535 power supply and a C4251 starter). The ITO working electrode was irradiated from behind with excitation light passed through a monochromator (Shimadzu, SPG-120S) (Figure 13). The reproducibility of all photocurrent properties was confirmed by performing at least duplicate measurements.

X-ray photoelectron spectroscopy (XPS): X-ray photoelectron spectra were obtained by using an X-ray photoelectron spectrometer (Kratos, AXIS 165) equipped with a monochromatic Al$_{K\alpha}$ source at 1486.6 eV. Take-off angles of 60° and 15° were adopted to observe the ITO surface species. The ITO samples were electrically contacted with the spectrometer and the charge was externally neutralized using a charge neutralizer (applied potential: 1.85 V) to avoid peak broadening and distortion. The binding energies were normalized to the residual C(1s) peak at 284.4 eV and the In(3d) peak at 443.9 eV attributable to In–O bonding. The peak profiles were deconvoluted by a Gaussian–Lorenztian (70:30) function. In the In(3d) and Sn(3d) regions, spin multiplicity was taken into consideration to fit multiplet splitting with a 3:2 population ratio for the 3d$_{5/2}$ and 3d$_{3/2}$ orbitals. In a similar way, a 2:1 population ratio for the Zn(2p$_{3/2}$) and Zn(2p$_{1/2}$) orbitals was applied for peak deconvolution.

[1] D. M. Adams, L. Brus, C. E. D. Chidsey, S. Creager, C. Creutz, C. R. Kagan, P. V. Kamat, M. Lieberman, S. Lindsey, R. A. Marcus, R. M. Metzger, M. E. Michel-Beyerle, J. R. Miller, M. D. Newton, D. R. Rolison, O. Sankey, K. S. Schanze, J. Yardley, X. Zhu, *J. Phys. Chem. B* **2003**, *107*, 6668.

[2] H. Ishii, K. Sugiyama, E. Ito, K. Seki, *Adv. Mater.* **1999**, *11*, 605.

[3] a) F. Nüesch, F. Rotzinger, L. Si-Ahmed, L. Zuppiroli, *Chem. Phys. Lett.* **1998**, *288*, 861; b) M. Carrara, N. Nüesch, L. Zuppiroli, *Synth. Met.* **2001**, *121*, 1633.

[4] X. Crispin, V. Geskin, A. Crispin, J. Comil, R. Lazzaroni, W. R. Salaneck, J.-L. Brédas, *J. Am. Chem. Soc.* **2002**, *124*, 8131.

[5] a) J. Guo, N. Koch, J. Schwartz, S. L. Bernasek, *J. Phys. Chem. B* **2005**, *109*, 3966; b) E. L. Hanson, J. Guo, N. Koch, J. Schwartz, S. Bernasek, *J. Am. Chem. Soc.* **2005**, *127*, 10058.

[6] a) S. Creager, C. J. Yu, C. Bamdad, S. O'Connor, T. MacLean, E. Lam, Y. Chong, G. T. Olsen, J. Luo, M. Gozin, J. F. Kayyem, *J. Am. Chem. Soc.* **1999**, *121*, 1059; b) H. D. Sikes, J. F. Smalley, S. P. Dudek, A. R. Cook, M. D. Newton, C. E. D. Chidsey, S. W. Feldberg, *Science* **2001**, *291*, 1519.

[7] A. A. Yasseri, D. Syomin, R. S. Loewe, J. S. Lindsey, F. Zaera, D. F. Bocian, *J. Am. Chem. Soc.* **2004**, *126*, 15603.

[8] SAMs on Au electrodes: a) K. Uosaki, T. Kondo, X.-Q. Zhang, M. Yanagida, *J. Am. Chem. Soc.* **1997**, *119*, 8367; b) H. Imahori, H. Norieda, H. Yamada, Y. Nisimura, I. Yamazaki, Y. Sakata, S. Fukuzumi, *J. Am. Chem. Soc.* **2001**, *123*, 100; c) K.-S. Kim, M.-S. Kang, H. Ma, A. K.-Y. Jen, *Chem. Mater.* **2004**, *16*, 5058.

[9] SAMs on ITO electrodes: a) H. Yamada, H. Imahori, Y. Nishimura, I. Yamazaki, T. K. Ahn, S. K. Kim, S. Fukuzumi, *J. Am. Chem. Soc.*

2003, *125*, 9129; b) H. Imahori, M. Kimura, K. Hosomizu, T. Sato, T. K. Ahn, S. K. Kim, D. Kim, Y. Nishimura, I. Yamazaki, Y. Araki, O. Ito, S. Fukuzumi, *Chem. Eur. J.* **2004**, *10*, 5111; c) Y.-J. Cho, T. K. Ahn, H. Song, K. S. Kim, C. Y. Lee, W. S. Seo, K. Lee, S. K. Kim, D. Kim, J. T. Park, *J. Am. Chem. Soc.* **2005**, *127*, 2380.

[10] Langmuir–Blodgett films: a) M. Fujihira, K. Nishiyama, H. Yamada, *Thin Solid Films* **1985**, *132*, 77; b) M. Fujihira, M. Sakomura, T. Kamei, *Thin Solid Films* **1989**, *180*, 43; c) A. Aoki, Y. Abe, T. Miyashita, *Langmuir* **1999**, *15*, 1463.

[11] Layer-by-layer membranes: a) C. Luo, D. M. Guldi, M. Maggini, E. Menna, S. Mondini, N. A. Kotov, M. Prato, *Angew. Chem.* **2000**, *112*, 4052; *Angew. Chem. Int. Ed.* **2000**, *39*, 3905; b) A. Ikeda, T. Hatano, S. Shinkai, T. Akiyama, S. Yamada, *J. Am. Chem. Soc.* **2001**, *123*, 4855; c) F. B. Abdelrazzaq, R. C. Kwong, M. E. Thompson, *J. Am. Chem. Soc.* **2002**, *124*, 4796; d) D. M. Guldi, I. Zilbermann, G. Anderson, A. Li, D. Balbinot, N. Jux, M. Hatzimarinaki, A. Hirsch, M. Prato, *Chem. Commun.* **2004**, 726; e) H. Furukawa, N. Inoue, T. Watanabe, K. Kuroda, *Langmuir* **2005**, *21*, 3992.

[12] S. M. Sze, *Physics of Semiconductor Devices*, 2nd ed., Wiley, New York, **1981**.

[13] P. Fromhelz, W. Arden, *J. Am. Chem. Soc.* **1980**, *102*, 6211.

[14] L. Sereno, J. J. Silber, L. Otero, M. del Valle Bohorquez, A. L. Moore, T. A. Moore, D. Gust, *J. Phys. Chem.* **1996**, *100*, 814.

[15] R. H. Wilson, *J. Appl. Phys.* **1977**, *48*, 4292.

[16] T. Miyasaka, T. Watanabe, A. Fujishima, K. Honda, *J. Am. Chem. Soc.* **1978**, *100*, 6657.

[17] A. Ulman, *Chem. Rev.* **1996**, *96*, 1533.

[18] a) T. J. Gardner, C. D. Frisbie, M. S. Wrighton, *J. Am. Chem. Soc.* **1995**, *117*, 6927; b) C. Yan, M. Zharnikov, A. Gölzhäuse, M. Grunze, *Langmuir* **2000**, *16*, 6208; c) B. Vercelli, G. Zotti, G. Schiavon, S. Zecchin, *Langmuir* **2003**, *19*, 9351.

[19] a) J. Deisenhofer, O. Epp, K. Miki, R. Huber, H. Michel, *J. Mol. Biol.* **1984**, *180*, 385; b) J. Deisenhofer, O. Epp, K. Miki, R. Huber, H. Michel, *Nature* **1985**, *318*, 618; c) J. Deisenhofer, H. Michel, *Science* **1989**, *245*, 1463; d) P. Allen, G. Feher, T. O. Yeates, D. C. Rees, J. Deisenhofer, H. Michel, R. Huber, *Proc. Natl. Acad. Sci. USA* **1986**, *83*, 8589.

[20] a) Y. Kobuke, H. Miyaji, *J. Am. Chem. Soc.* **1994**, *116*, 4111; b) Y. Kobuke, K. Ogawa, *Bull. Chem. Soc. Jpn.* **2003**, *76*, 689.

[21] H. Ozeki, A. Nomoto, K. Ogawa, Y. Kobuke, M. Murakami, K. Hosoda, M. Ohtani, S. Nakashima, H. Miyasaka, T. Okada, *Chem. Eur. J.* **2004**, *10*, 6393.

[22] M. Morisue, S. Yamatsu, N. Haruta, Y. Kobuke, *Chem. Eur. J.* **2005**, *11*, 5563.

[23] K. L. Purvis, G. Lu, J. Schwartz, S. L. Bernasek, *J. Am. Chem. Soc.* **2000**, *122*, 1808.

[24] a) I. Ichinose, H. Senzu, T. Kunitake, *Chem. Mater.* **1997**, *9*, 1296; b) I. Ichinose, T. Kawakami, T. Kunitake, *Adv. Mater.* **1998**, *10*, 535.

[25] a) J. B. Miller, J. Schwartz, S. L. Bernasek, *Langmuir* **1994**, *10*, 2629; b) S. K. Van der Kam, G. Lu, S. L. Bernasek, J. Schwartz, *J. Am. Chem. Soc.* **1997**, *119*, 11639; c) G. Lu, J. Schwartz, S. L. Bernasek, *Langmuir* **1998**, *14*, 1532.

[26] a) W. Göpel, J. A. Anderson, D. Frankel, M. Jaehnig, K. Phillips, J. A. Schäfer, G. Pocker, *Surface Sci.* **1984**, *139*, 333; b) S. Cherian, C. C. Wamser, *J. Phys. Chem. B* **2000**, *104*, 3624.

[27] a) T. Ishida, H. Kobayashi, Y. Nakano, *J. Appl. Phys.* **1993**, *73*, 4344; b) C. Donley, D. Dunphy, D. Paine, C. Carter, K. Nebesny, P. Lee, D. Alloway, N. R. Armstrong, *Langmuir* **2002**, *18*, 450.

[28] a) F. Cao, G. Oskam, P. C. Searson, J. M. Stipkala, T. A. Heimer, F. Farzad, G. J. Meyer, *J. Phys. Chem.* **1995**, *99*, 11974; b) R. L. Willis, C. Olson, B. O'Regan, T. Lutz, J. Nelson, J. R. Durrant, *J. Phys. Chem. B* **2002**, *106*, 7605.

[29] M. D. Porter, T. B. Bright, D. L. Allara, C. E. D. Chidsey, *J. Am. Chem. Soc.* **1987**, *109*, 3559.

[30] B. Vercelli, G. Zotti, G. Schiavon, S. Zecchin, *Langmuir* **2003**, *19*, 9351.

[31] a) A. Ghosh, *Acc. Chem. Res.* **1998**, *31*, 189; b) D. H. Karweuk, N. Winograd, *Inorg. Chem.* **1976**, *15*, 2336.

[32] N. Nishimura, M. Ooi, K. Shimazu, H. Fujii, K. Uosaki, *J. Electroanal. Chem.* **1999**, *473*, 75.

[33] F. Da Cruz, K. Driaf, C. Berthier, J.-M. Lameille, F. Armand, *Thin Solid Films* **1999**, *349*, 155.

[34] D. Kalita, M. Morisue, Y. Kobuke, *New J. Chem.* **2006**, *39*, 77.

[35] a) N. Mataga, H. Chosrowjan, Y. Shibata, N. Yoshida, A. Osuka, T. Kikuzawa, T. Okada, *J. Am. Chem. Soc.* **2001**, *123*, 12422; N. Mataga, S. Taniguchi, H. Chosrowjan, A. Osuka, K. Kurotobi, *Chem. Phys. Lett.* **2005**, *403*, 163; b) R. H. Hayes, C. J. Walsh, M. R. Wasielewski, *J. Phys. Chem. A* **2004**, *108*, 2375.

[36] a) H. S. Cho, D. H. Jeong, M.-C. Yoon, Y. H. Kim, Y.-R. Kim, D. Kim, S. C. Jeoung, S. K. Kim, N. Aratani, H. Shinmori, A. Osuka, *J. Phys. Chem. A* **2001**, *105*, 4200; b) S. Faure, C. Stern, R. Guilard, P. D. Harvey, *J. Am. Chem. Soc.* **2004**, *126*, 1253; c) T. Komatsu, M. Moritake, E. Tsuchida, *Chem. Eur. J.* **2003**, *9*, 4626.

[37] a) K. S. Kim, I. Park, S. Lee, K. Cho, J. Y. Lee, J. Kim, J. D. Joannopoulos, *Phys. Rev. Lett.* **1996**, *76*, 956; b) L. Kevan, *Acc. Chem. Res.* **1981**, *14*, 138; c) J. R. R. Verlet, A. E. Bragg, A. Kammrath, O. Cheshnovsky, D. M. Neumark, *Science* **2005**, *307*, 93.

[38] a) C. Zimmermann, F. Willig, S. Ramakrishna, B. Burfeindt, B. Pettinger, R. Eichberger, W. Storck, *J. Phys. Chem. B* **2001**, *105*, 9245; b) J. Schnadt, P. A. Brühwiler, L. Patthey, J. N. O'Shea, S. Södergen, M. Odelius, R. Ahuja, O. Karis, M. Bässler, P. Persson, H. Siegbahn, S. Lunell, N. Mårtensson, *Nature* **2002**, *418*, 620; c) K. Onda, B. Li, J. Zhao, K. D. Jordan, J. Yang, H. Petek, *Science* **2005**, *308*, 1154.

[39] J. M. Bolts, M. S. Wrighton, *J. Phys. Chem.* **1976**, *80*, 2641.

[40] a) Y. Sato, M. Fujita, F. Mizutani, K. Uosaki, *J. Electroanal. Chem.* **1996**, *409*, 145; b) M. Y. Okamura, M. L. Paddock, M. S. Graige, G. Feher, *Biochim. Biophys. Acta* **2000**, *1458*, 148; c) H.-G. Hong, W. Park, *Langmuir* **2001**, *17*, 2485.

[41] F. Nüesch, L. J. Rothberg, F. W. Forsythe, Q. T. Le, Y. Gao, *Appl. Phys. Lett.* **1999**, *74*, 880.

[42] D. F. Watson, A. Marton, A. M. Stux, G. J. Meyer, *J. Phys. Chem. B* **2004**, *108*, 11680.

[43] a) F. Odobel, E. Blart, M. Lagree, M. Villieras, H. Boujtita, N. El Murr, S. Caramori, C. A. Bignozzi, *J. Mater. Chem.* **2003**, *13*, 502; b) W. M. Campbell, A. K. Burrell, D. L. Officer, K. W. Jolley, *Coord. Chem. Rev.* **2004**, *248*, 1363.

[44] a) B. Choudhury, A. C. Weedon, J. R. Bolton, *Langmuir* **1998**, *14*, 6199; b) H. Imahori, T. Hasobe, H. Yamada, Y. Nishimura, I. Yamazaki, S. Fukuzumi, *Langmuir* **2001**, *17*, 4925.

[45] A. Ohashi, A. Satake, Y. Kobuke, *Bull. Chem. Soc. Jpn.* **2004**, *77*, 365.

[46] T. Hirao, T. Masunaga, Y. Ohshiro, T. Agawa, *Synthesis* **1981**, 56.

[47] a) R. Rabinowitz, *J. Org. Chem.* **1963**, *28*, 2975; b) D. Deniaud, B. Schöllorn, D. Mansuy, J. Rouxel, P. Battioni, B. Bujoli, *Chem. Mater.* **1995**, *7*, 995.

[48] W. Fudickar, J. Zimmermann, L. Ruhlmann, J. Schneider, B. Röder, U. Siggel, J.-H. Furhop, *J. Am. Chem. Soc.* **1999**, *121*, 9539.

[49] E. Díez-Barra, J. C. García-Martínez, S. Merino, R. del Rey, J. Rodríguez-López, P. Sánchez-Verdú, J. Tejeda, *J. Org. Chem.* **2001**, *66*, 5664.

[50] T. J. Meyer, G. J. Meyer, B. W. Pfennig, J. R. Schoonover, C. J. Timpson, J. F. Wall, C. Kobusch, X. Chen, B. M. Peek, C. G. Wall, W. Ou, B. W. Erickson, C. A. Bignozzi, *Inorg. Chem.* **1994**, *33*, 3952.

[51] J. M. Tour, L. Jones, II, D. L. Pearson, J. J. S. Lamba, T. P. Burgin, G. M. Whitesides, D. L. Allara, A. N. Parikh, S. V. Atre, *J. Am. Chem. Soc.* **1995**, *117*, 9529.

Please note: Minor changes have been made to this manuscript since its publication in *Chemistry—A European Journal* Early View. The Editor.